The Distribution of Ion Acceptance in Atmospheric Pressure Ion Sources: Spatially Resolved APLI Measurements

Matthias Lorenz, Ralf Schiewek, Klaus J. Brockmann, Oliver J. Schmitz, Siegmar Gäb, and Thorsten Benter

Department of Chemistry, University of Wuppertal, Wuppertal, Germany

It is demonstrated that spatially resolved mass selected analysis using atmospheric pressure laser ionization mass spectrometry (APLI MS) represents a new powerful tool for mechanistic studies of ion-molecule chemistry occurring within atmospheric pressure (AP) ion sources as well as for evaluation and optimization of ion source performance. A focused low-energy UV laser beam is positioned computer controlled orthogonally on a two-dimensional grid in the ion source enclosure. Resonance enhanced multiphoton ionization (REMPI) of selected analytes occurs only within the confined volume of the laser beam. Depending on the experimental conditions and the reactivity of the primary photo-generated ions, specific signal patterns become visible after data treatment, as visualized in, e.g., contour or pseudo-color plots. The resulting spatial dependence of sensitivity is defined in this context as the distribution of ion acceptance (DIA) of the source/analyzer combination. This approach provides a much more detailed analysis of the diverse processes occurring in AP ion sources compared with conventional bulk signal response measurements. (J Am Soc Mass Spectrom 2008, 19, 400–410) © 2008 American Society for Mass Spectrometry

The suite of the most widely used atmospheric pressure ionization (API) techniques for coupling with liquid chromatography (LC), i.e., electrospray ionization (ESI), atmospheric pressure chemical ionization (APCI), and atmospheric pressure photo ionization (APPI) [1–6], has been recently complemented with a fourth technique, atmospheric pressure laser ionization (APLI) [7–11]. Whereas ESI and APCI cover the strong to medium polarity analyte range, respectively, APPI was originally proposed to close the hitherto existing low-polarity gap [12, 13]. Despite the promise of highly efficient *direct* one-photon ionization of low polarity analytes by vacuum ultra-violet (VUV) radiation to yield parent radical cations (eq 1), rather poor detection limits were reported [14–17].

$$M + h\nu \rightarrow M^{\cdot+} + e^{-} \left(\text{e.g., } \lambda = 124\ \text{nm; } E = 10\ \text{eV}\right) \quad (1)$$

Instead, particularly upon APPI MS analysis of compounds exhibiting elevated gas-phase basicities, predominantly formation of quasimolecular ions ($[M + H]^+$) was observed [18]. Consequently, in the majority of reports on the analytical application of APPI, a variation of the technique is applied: a dopant is added in considerable amounts (approaching liquid phase mixing ratios of several percent) to the liquid flow entering the vaporization stage, resulting in dopant assisted APPI (DA APPI) [15]. After pneumatically assisted vaporization of the liquid mixture within the heated AP probe, the dopant is present in large excess over the analyte(s) in the gas phase and, despite the low direct ionization efficiency, substantial amounts of dopant ions are generated (eq 2). Subsequent proton transfer reactions, provided favorable thermodynamic conditions exist, may then result in quasimolecular ion formation:

$$D + h\nu \rightarrow D^{\cdot+} \left(\lambda = 124\ \text{nm; } E = 10\ \text{eV}\right) \quad (2)$$

$$D^{\cdot+} + M \rightarrow \left[M + H\right]^+ + \left[D - H\right]^{\cdot} \quad (3)$$

The proposed mechanism is far more complex than shown here, in particular with respect to the protonating agent, as was discussed in the literature [14, 16, 17, 19–23]. All available data suggest that the LC solvents, e.g., acetonitrile (CH_3CN), methanol (CH_3OH), or H_2O, are directly involved in the subsequent ion-molecule chemistry following the ionization of the dopant. Upon formation of clusters of variable size and thus gas phase acidity, these species are considered as the protonating agents:

$$D^{\cdot+} + S_n \rightarrow \left[D^{\cdot+} \cdot n\,S\right] \quad (4)$$

$$\left[D^{\cdot+} \cdot n\,S\right] \rightarrow \left[D - H\right]^{\cdot} + \left[\left[S + H\right] \cdot \left(n - 1\right) S\right]^+ \quad (5)$$

In contrast hereto, using APLI under otherwise identical conditions as in direct APPI, i.e., in the absence of

Address reprint requests to Dr. Thorsten Benter, Department of Chemistry, University of Wuppertal, Gauss Str. 20, D-42119 Wuppertal, Germany. E-mail: tbenter@uni-wuppertal.de

1044-0305/08/$32.00
doi:10.1016/j.jasms.2007.11.021

Published online December 8, 2007
Received May 30, 2007
Revised November 27, 2007
Accepted November 27, 2007

any dopant, in many cases efficient formation of radical cations is observed. In addition, the sensitivity for non- to very low-polar aromatic or highly conjugated compounds is up to three orders of magnitude higher compared with APPI [9–11, 21]. Currently, APLI outperforms all other API techniques for measurement of polycyclic aromatic hydrocarbons (PAH) with respect to sensitivity and detection limits. This was not expected, particularly in comparison with the performance of APPI. In the latter case, only the duty cycle of the mass spectrometer is a major limiting factor of the data acquisition since a continuously radiating VUV lamp is used for ionization. Typical duty cycles for quadrupole time of flight (Q-TOF) hybrid MS are 5% to 30% [24]. With APLI, the pulsed laser system severely limits the achievable performance: at repetition rates of typically 200 Hz and a pulse duration of about 10 ns, the duty cycle is only 1.6×10^{-6} with respect to average ionization time.

These surprising results are the motivation for the present investigation. APLI is based on (1 + 1) REMPI at low laser power densities about 1 MW cm^{-2} and is thus specific towards ionization of aromatic hydrocarbons:

$$M\left(S_0\right) + h\nu \rightarrow M^*\left(S_{1,2,3,\ldots}\right) \quad (6a)$$

$$M^*\left(S_{1,2,3,\ldots}\right) + h\nu \rightarrow M^{\cdot+} + e^- \quad \left(\text{e.g., } \lambda = 248 \text{ nm; } E_{total} = 2 \times 5 \text{ eV}\right) \quad (6b)$$

As discussed before [7, 10] this sphericity arises mainly from the spectroscopic features of aromatic hydrocarbons as well as from the experimental conditions generally prevailing in API MS: (1) the cross sections of aromatic hydrocarbons, particularly of systems consisting of more than one conjugated ring such as PAH, are generally high at 248 nm. (2) Generally, *bound* intermediate states of the type S_n ($n = 1, 2, 3 \ldots$) exist for these compound classes that allow for excitations with favorable transition probabilities. Systems with more than one conjugated ring are generally ionized via excitation of higher singlet states; here, the density of states increases significantly compared with the S_1 regime – this is also manifest in the respective UV absorption spectra. (3) The elevated temperature of up to 350 °C in the AP analyte delivery stage broadens the spectral rovibrational absorption features of the $S_n \leftarrow S_0$ band systems to an extent that numerous resonant transitions are realized with 248 nm radiation. (4) The ionization potential is generally below 10 eV (some exceptions are, e.g., heavily fluorinated compounds). (5) Under such conditions, the laser power density is favorably adjusted to values close to the threshold of REMPI, which is about 10^5–10^6 W cm^{-2}. Hardly any other compound class ionizes efficiently under such conditions; at the same time, higher order REMPI processes are strongly suppressed (e.g., (2 + 1) REMPI of solvents). Furthermore, the high pressure prevailing in the ionization region strongly suppresses ionic fragmentation since the collision rate of excited parent ions with the bath gas N_2 is favorably competing with unimolecular decomposition rates. There are a few exceptions to these general observations; if for example the presence of functional groups attached to the aromatic system strongly promotes intramolecular relaxation- or molecular dissociation processes (for the latter, e.g., nitro groups), the loss of excited molecules from the resonantly pumped S_n intermediate state leads to weak or even absent ion signals. However, vast numbers of aromatic hydrocarbons have been successfully detected with REMPI; see references [7, 25–27] for details.

It is pointed out that even under drastically enhanced laser power densities up to 10^{10} W cm^{-2} fragmentation is hardly observed in APLI; for several unsubstituted PAH power densities up to 10^{12} W cm^{-2} did not generate any fragment ions (data obtained using a high power excimer laser, results not shown here). Thus, individual APLI mass spectra of the present compounds consist of their molecular or quasi-molecular ion signals only.

With reference to eqs 6a and b, clearly both photo ionization techniques, APPI as well as APLI, should at least result in identical *primary* ion generation independent of single- (eq 1) or two-step ionization. Upon single step VUV ionization in collision free environments, this is in fact the case [28, 29]. This strongly suggests that matrix compounds are actively participating in secondary parent radical ion-molecule chemistry before expansion into the collision free environment of the analyzer.

Experimental

Methods and Instrumentation

API source and MS. All experiments are performed with a MicroMass Q-TOF Ultima II orthogonal time of flight mass spectrometer (Waters GmbH, Eschborn, Germany) running in full scan mode with a scan time of 1 s covering the mass range *m/z* (100–1000) resulting in about 28,000 time-to-digital converter (TDC) sweeps per scan. The original MicroMass APCI/APPI Z-Spray source enclosure was replaced by a home-built combined APCI/APLI/APPI stage, as shown in the diagram in Figure 1a; Figure 1b shows a photograph covering the area outlined red in the drawing. Two fused silica windows with 4 and 2 cm diameters mounted on top and bottom of the source enclosure serve as laser beam entry and exit, respectively. For routine APLI operation the diameter of the upper window is usually as small as the lower one; however, in the present investigation the beam is scanned across a relatively large area in the source, see below. The main gas flow entering the AP source consists of vaporized liquids as well as make-up gases that are added (1) inside the heater and (2) through an additional entrance coaxially surrounding the heater's exit, which are both visible in the lower section in Figure 1b. The MS sampling nozzle is located on the left. A pumping

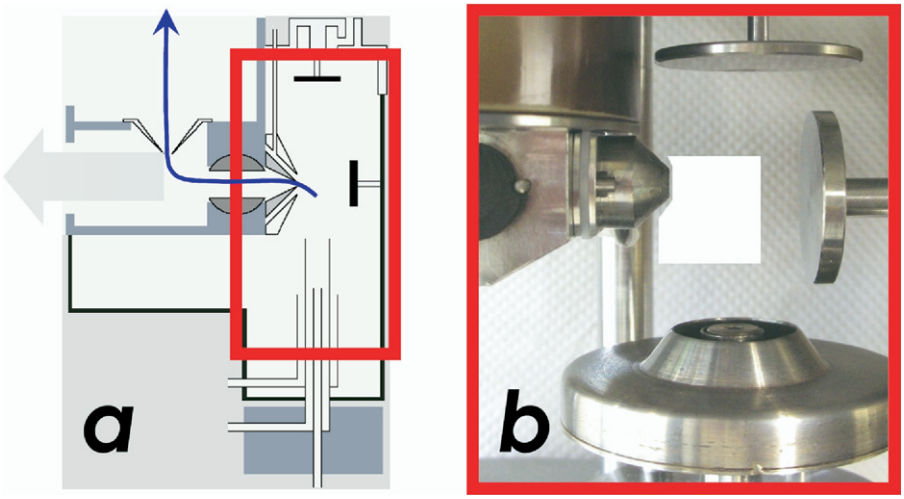

Figure 1. Diagram (**a**) and photograph (**b**) of the MicroMass AP ion source used in the present investigations. Gray arrow: Main flow of neutrals. Blue arrow: Ion trajectory. For details see text.

speed of about 200 L h^{-1} is measured directly at the nozzle with a calibrated FM-360 mass flow meter (Tylan GmbH, Munich, Germany) and corresponds to the expected flow by effusion through a leak of 0.36 mm^2 from an atmospheric into a low-pressure region, according to the present MS sampling orifice area. In all experiments, the total gas flow leaving the heater always exceeds the pumping speed at the sampling orifice; the excess is swept out of the source via an exhaust line connected to a vent at ambient pressure. The nebulizer gas flow is set to 150 L h^{-1} with a 500 L h^{-1} calibrated flow meter (Krohne GmbH, Duisburg, Germany); the desolvation gas flow of 150 L h^{-1} is adjusted by means of the instrument's embedded flow meter. In the present experiments both, the nebulizer and the desolvation gas flow supply is dry nitrogen from compressed gas cylinders with a stated purity of 99.9995% vol. (Air Liquide GmbH, Düsseldorf, Germany). The liquid flow delivered to the heater with an Hitachi L-7110 HPLC pump (Hitachi Ltd., Tokyo, Japan) is set to 300 μL min^{-1}, resulting in an additional gas flow after complete vaporization of about 8 L h^{-1}, as calculated with the ideal gas law. The heater temperature is set to 300 °C, the MS ion block is held at 150 °C. The repeller electrode (cf. reference [7]) as seen on the right side of Figure 1b, or alternatively the face ring of the APPI lamp housing is biased between 0 to 200 V. This set-up creates an additional ion guiding electrical field gradient, which is intrinsically present in ESI and APCI but not in APPI and APLI. It was shown earlier that installation of an additional repeller electrode significantly enhances the performance of the present APLI source [7]. Pulsed laser light is obtained from an Optex excimer laser (Lambda Physik, Göttingen, Germany) with a pulse length of about 10 ns (FWHM).

Computer controlled laser beam steering stage. For routine APLI operation the unfocused excimer laser beam with a pulse energy of 10 mJ delivered on an area of about 1 cm^2 within 8 ns and 100 to 200 Hz repetition rate is favorably used. The resulting power density of roughly 1 MW cm^{-2} is close to the lower threshold for efficient (1 + 1) REMPI; however, under these conditions ionic fragmentation is not observed, see above [7, 9, 10]. In the present experiments, a mildly attenuated laser beam passes an iris with an aperture of 5 mm and is focused with a fused silica lens of 125 mm nominal focal length and 25.4 mm diameter to achieve spatial scanning in the x,y-plane perpendicular to the light propagation direction (cf. Results and Discussion sections for further details). The resulting pulse energy of the light entering the ionization source was 2.0 mJ. The smallest suitable focal length of the lens is determined by the minimum distance between the x,y-positioning stage and the ion sampling region of the source. Using this set-up, the focused laser beam is easily positioned by moving the lens in the x,y-plane (and thus the focal point), which determines the further propagation of the entering essentially parallel beam, as depicted in Figure 2a. A custom-built x,y-lens positioning stage equipped with computer controlled stepping motors (Fuji Co., Tokyo, Japan) is employed. A home-built interface connects the controlling computer and the stepping motor driving unit. The spatial resolution in the plane perpendicular to the nozzle orifice is about 0.1 mm per individual motor step. It is shown further below that step sizes about 1 mm generate sufficiently resolved data for the present investigation. Other configurations using non-focusing optics with multiple mirrors are conceivable; however, for the present initial experiments the simple approach as described above is employed.

Data treatment. Full mass spectra are recorded at each grid point. For data treatment and analysis, individual mass traces as obtained from the MS data analysis software are transferred to the custom data treatment software. In the present experiments the integration range was set to $\Delta m \pm 0.5$ of the ion signal of interest.

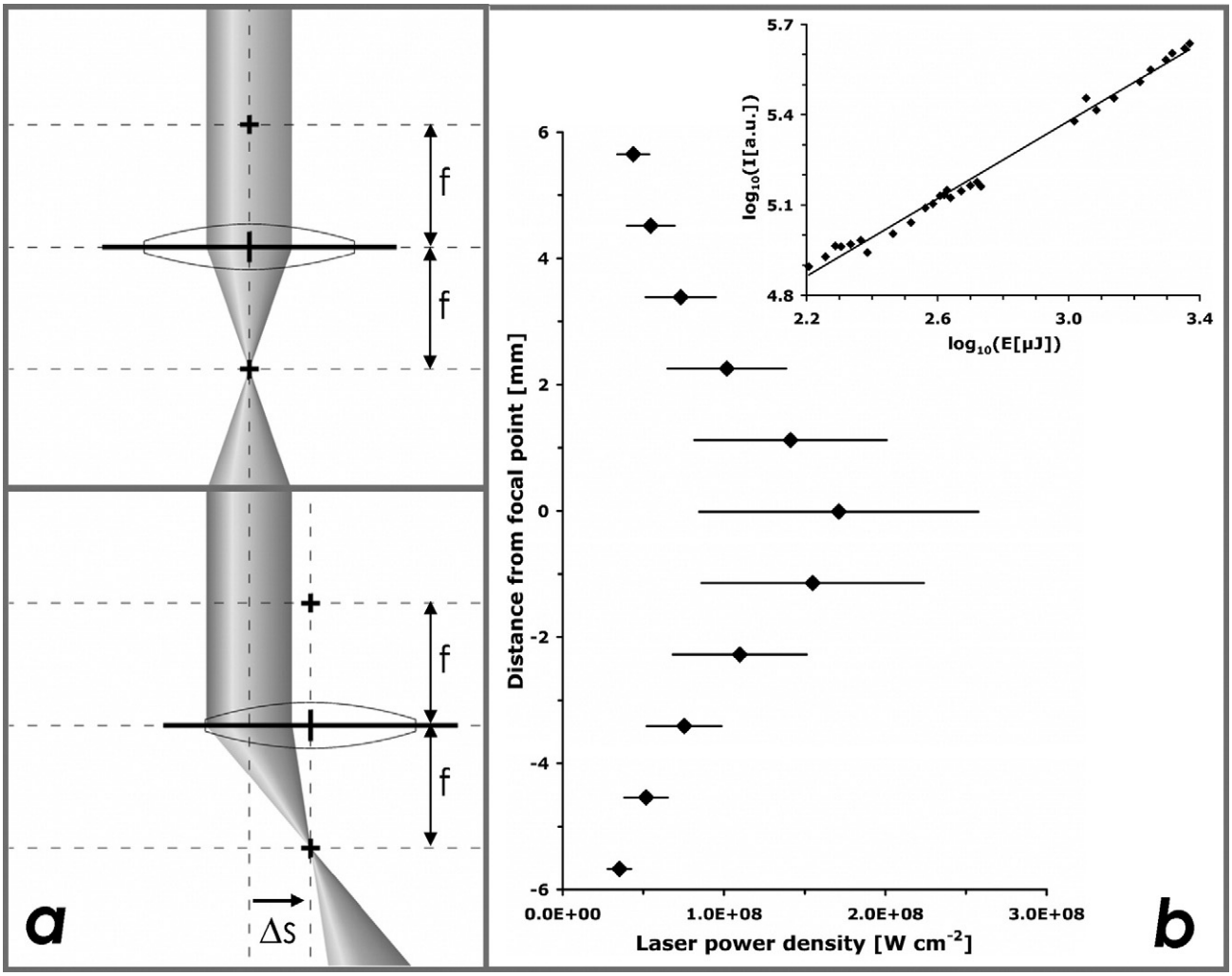

Figure 2. (**a**) Diagram of the optical set-up used for adjusting the laser focus position within the AP ion source (f = focal length of the lens, Δs = displacement of the focus position from the optical axis). (**b**) Plot of the laser power density versus distance from focal plane as calculated from the measured laser ablated area and laser pulse energy (see text). Insert: Power dependence of the radical cation signal intensity of B*a*P in double logarithmic representation. Note: All DIA measurements discussed here were run at 2.0 mJ pulse energy, i.e., 3.3 on the abscissa.

Figure 3 shows schematically the raw data treatment procedure. The resulting three-dimensional data arrays containing the relative x- and y-position of the lens, and the mass selected integrated ion signal intensity are presented as either contour or pseudo-color plots.

Software. A simple user interface that allows the reproducible positioning of the lens was written as a standalone software application running on a personal computer with DOS as operating system. It controls the stepping motor driving unit via the parallel I/O port by means of predefined scan files. The positioning of the translational stage is used as a virtual x-, y-, time-reference coordinate system. The position-time correlation is used to process the temporal signal profiles recorded by the MS software during the scanning process. For this purpose a custom program written in Matlab is used. Mass traces for the ions of interest are extracted from the signal profiles. Using as input both, the scan files that control the x-, y-, time-positioning of the optical stage and the mass traces containing the signal-time correlation, the program calculates and displays the corresponding DIA with respect to the x,y-reference coordination system.

Chemicals. CH_3CN, *n*-heptane, fluorene (1), benzo[*a*]pyrene (B*a*P (2)), 7,9-dimethylbenz[*c*]acridine (DMBA (3)), and nicotine (4) were obtained from Sigma-Aldrich GmbH, Seelze, Germany; structures are shown in Figure 4). Toluene was purchased from Merck KGaA, Darmstadt, Germany. All solvents were of chromatographic or analytical purity, and all other chemicals were of the highest purity available and used without further treatment.

1 mmol L^{-1} stock solutions of (1)–(4) dissolved in CH_3CN or *n*-heptane, respectively, were further diluted to the appropriate concentration in individual runs;

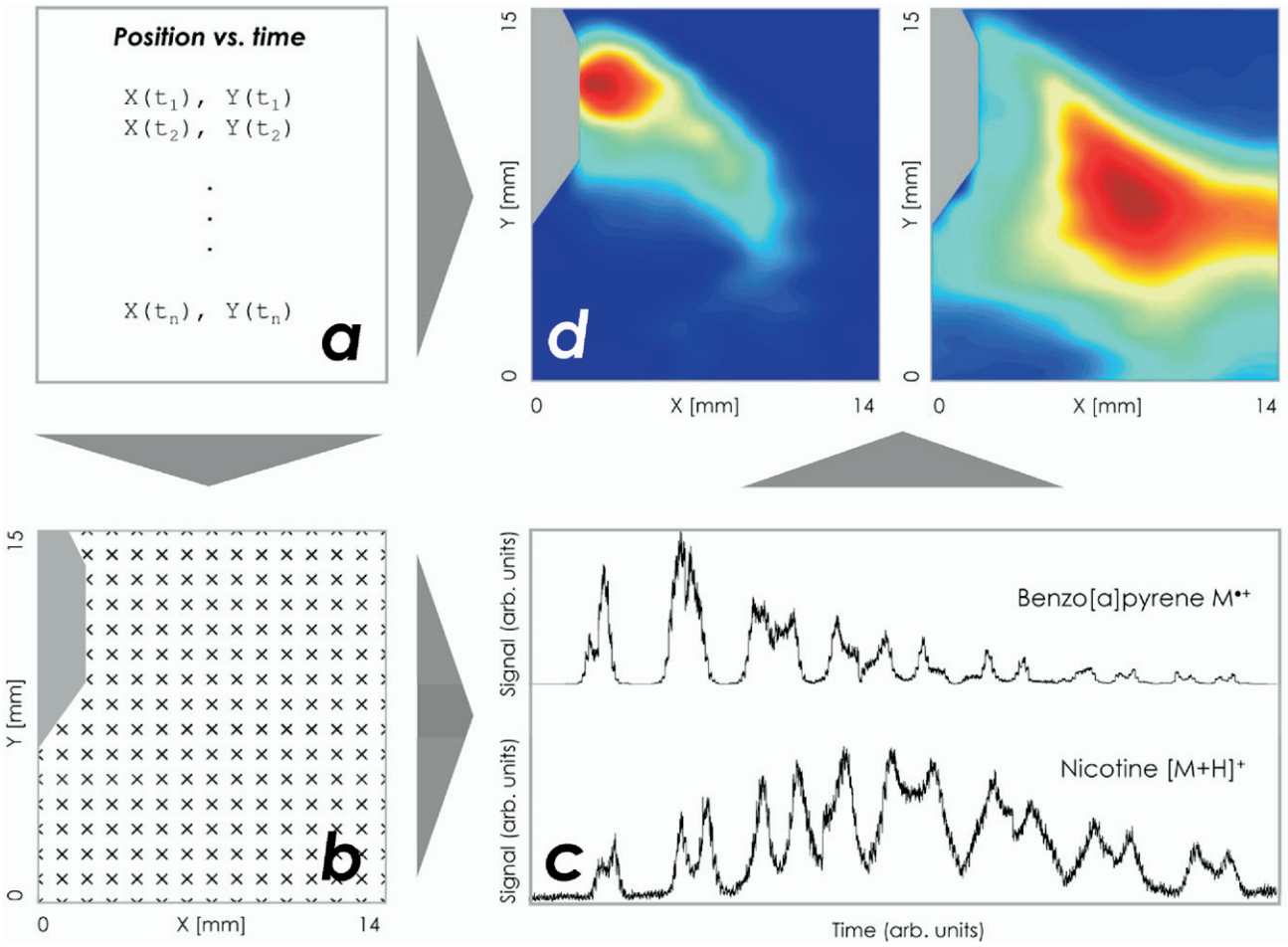

Figure 3. Schematic representation of the DIA measurement procedure, resulting raw data and data processing. The position-time correlation provided by the scan files (**a**) is used to control the optical stage and move the laser between spatially defined grid points in the AP ion source (**b**). The resulting temporal ion signal profiles are extracted as mass traces (**c**); together with the scan file data and the relative position of the x,y,z-coordinate system within the source the mass traces can be interpreted as DIA (**d**).

typical analyte concentrations were 1 to10 μmol L^{-1}. In some experiments, mixtures of analytes were also used. For dopant assisted APLI experiments, up to 2% (by volume) of toluene was added to the solution containing the analyte(s).

Results

As briefly discussed above, several independent parameters are impacting on the probability that a primarily generated ion reaches the detector and registers as a measurable signal. We refer to the resulting apparent relative sensitivity changes within the source enclosure as the *DIA* of the analyzer. In this paper, we are concerned about processes occurring at elevated pressure prevailing in the source enclosure. Within this framework, it is simply assumed that ions moving downstream of the sample cone are detected with a probability that is orders of magnitude higher than that of ions on passage upstream the cone. (This is certainly not entirely true, particularly for the "Z-Spray" geometry of the ion source employed. It is conceivable that the local pressure in the differentially pumped chamber of the MS inlet still corresponds to mean free paths of the ions and neutrals which is far less than the chamber dimensions. After passage through the second skimmer, a collision-free environment can be safely assumed). The largest forces impacting on the ion trajectories are generated (1) by fluid flow dynamics, i.e., elastic, nonreactive collisions of ions with neutrals. and (2) the electrical field gradient. The primary ion signal intensity may be further strongly affected by (3) ion-molecule reactions (reactive collisions) and thus also by the position and spatial extension of the origin of primary ion production. The amount of radical cations primarily formed in APLI depends on the concentration of analyte molecules within the irradiated volume and their interaction with the laser radiation.

Conventional API methods have no or only very restricted means of dynamically changing the origin of primary ion production: The corona discharge region in APCI is located around the needle tip; changing the

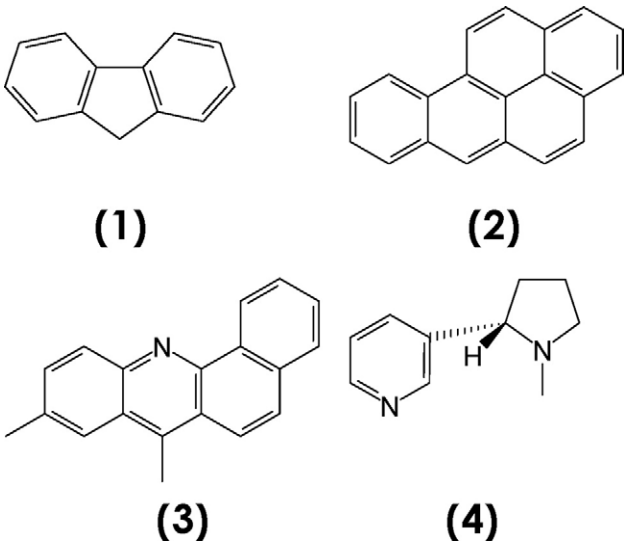

Figure 4. Chemical structures of the four analytes employed in the present investigation.

needle position influences several parameters simultaneously. Most pronounced is a significant change of the electrical field gradient and discharge current within the source enclosure. The same arguments apply for ESI. The VUV lamp in APPI is usually too bulky for in situ changes of the geometry; furthermore, primary ion production is restricted to a region of very small distance to the VUV light exit window. This is mainly caused by the strong absorption of matrix compounds, as will be discussed below.

In APLI the primary ion formation is completely separated from any other ion source parameters and essentially independent from electrical field gradients present. In contrast to the 124 nm VUV light often used in APPI, the penetration depth of 248 nm laser radiation in the source enclosure is basically unrestricted (the following discussion also applies to VUV laser excitation, e.g., with 118 nm radiation from a frequency tripled third harmonic of a Nd:YAG laser): At 124 (118) nm the cross sections of typical solvents used in LC-MS such as CH_3OH, CH_3CN, *n*-heptane, H_2O, and most others, are about 10^{-17} cm^2 molecule^{-1} [30–35]. *Typical* flow rates used in LC-MS when applying pneumatically assisted vaporization stages are around 200 μL min^{-1} liquid solution flow, and 300 L h^{-1} total N_2 (i.e., nebulization and desolvation) gas flow. We assume that a 1 μmol L^{-1} B*a*P solution is quantitatively vaporized at a heater temperature of 350 °C, all gases behave ideally, and the effluent from the vaporizer enters the source enclosure through an area of about 1 cm^2, creating a cylinder in which the gases propagate toward the MS sampling nozzle (all these assumptions, particularly the latter, are certainly not valid). Using the ideal gas law and assuming a vapor temperature of 140 °C and a total pressure of 1 bar, the number densities of N_2, CH_3CN (*n*-heptane), and analyte are calculated to be 1.8×10^{19}, 4.4×10^{17} (1.6×10^{17}), and 2.4×10^{10} molecule cm^{-3}, respectively.

Note that Cristoni et al. [36] measured a temperature of 135–145 °C for vaporized solvents in N_2 applying up to 30 μL min^{-1} liquid and 2.5 L min^{-1} N_2 flow, and 400 °C nebulizer temperature. It follows that a gas temperature of 140 °C is a reasonable upper limit for the present conditions. Applying Beer-Lambert's Law and using an absorption cross section of 3×10^{-17} cm^2 molecule^{-1} for CH_3CN [34] (7×10^{-17} cm^2 molecule^{-1} for *n*-heptane [35] at 124 nm, we calculate that the light intensity has dropped to roughly 2% after traveling 3 mm (3.5 mm) within the modeled gas flow cylinder. At 248 nm however, only linear and/or nonlinear absorption processes by the *analytes present* lead to light intensity attenuation. Bulk gases as well as vaporized solvents are generally transparent at this wavelength; higher order REMPI processes have been already discussed before. Since the analytes are present in trace amounts only, the photon flux is assumed to be constant within the propagation direction of the laser beam. Similar considerations apply for the dopant as far as it is added in *moderate* amounts of a few percent per volume liquid flow.

The DIA Data Evaluation

The white colored area in Figure 1b represents the 14×15 mm^2 region scanned with a grid spacing of 1 mm in each direction. Although the smallest step size resulting from one individual motor step is much smaller (see Experimental section), this spacing is chosen to reduce the amount of data acquired as well as the time needed for an entire DIA scan consisting of about 220 grid points. This resolution appears to be sufficient to yield reliable interpolation data. Consequently, the total time required for one experimental run covering the entire DIA scan area is about 80 min. Obviously it is of paramount importance for DIA measurements that the concentration of the analyte within the sampling region is kept constant for the entire length of one scan. Corresponding experiments have shown a very good reproducibility of DIA measurements.

In the experiments the highest photon density of the laser beam is expected within the Rayleigh region as an almost cylindrical volume element. This implies the possibility to restrict ion formation to occur only within this confined volume by properly adjusting the light intensity. For the present optical system, the Rayleigh length is calculated to be about 40 μm with a beam waist of 2 μm within this region, based on the assumption of far field conditions for a Gaussian laser beam profile [37, 38]. However, since it is notoriously difficult to calculate the properties of an excimer laser beam (none of the above assumptions are valid) we have experimentally determined these critical beam parameters. Upon exposing an anodized black metal surface to the attenuated laser beam at various lens–surface distances, the minimum ablated area measured using a calibrated microscope was 0.2×0.2 mm^2. This area is only remotely representing the beam waist dimensions

since the threshold level for quantitative ablation of the black surface layer is unknown. Figure 2b shows a plot of the laser power density as calculated using the measured pulse energy and a pulse duration of 8 ns versus distance from the focal point. Within distances of ±5 mm from the focal plane, i.e., the maximum of the curve, the laser power density roughly changes only by a factor of 5. Furthermore, the insert in Figure 2 shows the power dependency of the parent ion signal of B*a*P in double logarithmic presentation. The slope of the curve is about 0.6 over a comparable power density range as used here, clearly indicating kinetic saturation of the ionization step. This is in full accord with the rate model developed by Zakheim and Johnson [39]. Due to the very large absorption *and* ionization cross sections of B*a*P, the model predicts significant kinetic saturation to occur under the present experimental conditions, as observed. This means that a restriction of the ionization volume to a finite volume element in the present set-up is not possible. It thus follows that all DIA data presented here are projections of the integral ion signal intensity within the laser irradiated volume (cf. Figure 2) on the x,y-plane, which has its origin at z = 0, i.e., the nozzle orifice.

DIA Measurements and Definition of the Dynamic Ion Acceptance Volume (DIAV)

Before we begin with the interpretation of experimental data, we define DIA as well as DIAV in the following paragraphs. We refer to the following values: (x,y) denotes a position on the scanned grid inside the source enclosure $I_a(x,y)$ is the sum of ion signals I_α for all ion species α that are generated upon ionization of the analyte recorded at the position (x,y), or the total ion signal (TIS). The TIS belongs to one specific analyte. This differs from the total ion count (TIC) in a mass spectrum if other signals not originating from the analyte are also present. The TIS for one analyte may consist of contributions from radical cations, quasimolecular ions, fragments, etc. In APLI, for most analytes (e.g., PAH), only parent radical ions are generated, for others, (e.g., nicotine or DMBA), formation of radical cations as well as quasimolecular ions are observed; in other terms these ions *contribute* to the DIAV of the analyte. Fragmentation is generally not observed in APLI, but may in some special cases; we have thus included the potential presence of such signals in the DIAV definition, as given below.

The term DIA relates to the nature of the experiment rather than to an analytical figure of merit. The result of a DIA measurement is a set of experimental data that consists of accumulated mass spectra for each selected laser beam position. After data treatment, the recorded TIS is plotted as function of the two spatial coordinates resulting in a contour plot (single ion signals, i.e., the individual contributions to the DIAV, may be extracted after data treatment). This plot represents the distribution of the product of ion yield and the overall transmission efficiency from the point of origin of ion formation (i.e., the laser irradiated volume) to the detector. The transmission efficiency is affected by a number of external parameters, which may be adjustable (electrical potentials as well as gas flows), or which are hardly controllable, if at all (e.g., ion-molecule reaction rates, presence of reactive trace compounds in the bulk gases and solvents).

The ion acceptance volume defines an analytical figure of merit, which is calculated from the results of DIA measurements. To demonstrate the dynamic behavior of this volume, we use the term DIAV. The boundaries of this volume are calculated from a complete DIA scan: the volume element under consideration, V(x,y), belongs to the DIAV if the TIS recorded at this position is larger than 1/e of the maximum of *all* recorded TIS generated in an entire DIA scan. As already mentioned above, the individual contributions to the DIAV may be extracted from DIA scans; in this case single ion signals are scaled against the max. TIS as described above.

Interpretation of DIA Measurements

Upon nebulizing a 1 μmol L^{-1} solution of fluorene as representative of the PAH compound class, typical graphs as shown in Figure 5 are obtained (*m/z* 166; corresponding to $M^{\cdot+}$ of fluorene). The scanned region matches the white colored area in Figure 1b. From left to right, the repeller voltage was increased from 0 to +200 V. All other PAH investigated so far (compounds containing 2 to 5 condensed aromatic rings) show qualitatively the same behavior. A couple of crucial conclusions can be readily drawn from the data. First, radical cations are only "visible" to the detector within a few mm away from the sampling orifice. Second, the plots show clearly that the mass spectrometer accepts ions from a larger volume at higher repeller potentials. Upon further increasing the voltage, no growth of the DIAV is observed. Results not shown here demonstrate that the individual gas flows in the vaporization stage, i.e., nebulizer, desolvation, and cone gas flows, have a pronounced impact on the shape of the DIAV, as expected from bulk ion intensity measurements.

In contrast hereto, the contribution of quasimolecular ions to the DIAV generally extends much further into the ion source compared with the contributions of radical cations; in fact quasimolecular ions generally determine the shape of the DIAV. As illustration, spatially resolved measurements of DMBA were performed. It is reasonable to assume that DMBA exhibits a high gas-phase basicity that is comparable to that of acridine (940.7 kJ mol^{-1}) [40]. Upon vaporizing a 10 μmol L^{-1} solution of DMBA dissolved in *n*-heptane both, radical cations as well as quasimolecular ions are formed with APLI. The origin of the latter is discussed below. The spatially resolved measurements reveal that (1) the area of maximum signal intensity for both species appears to be separated, (2) radical cations are

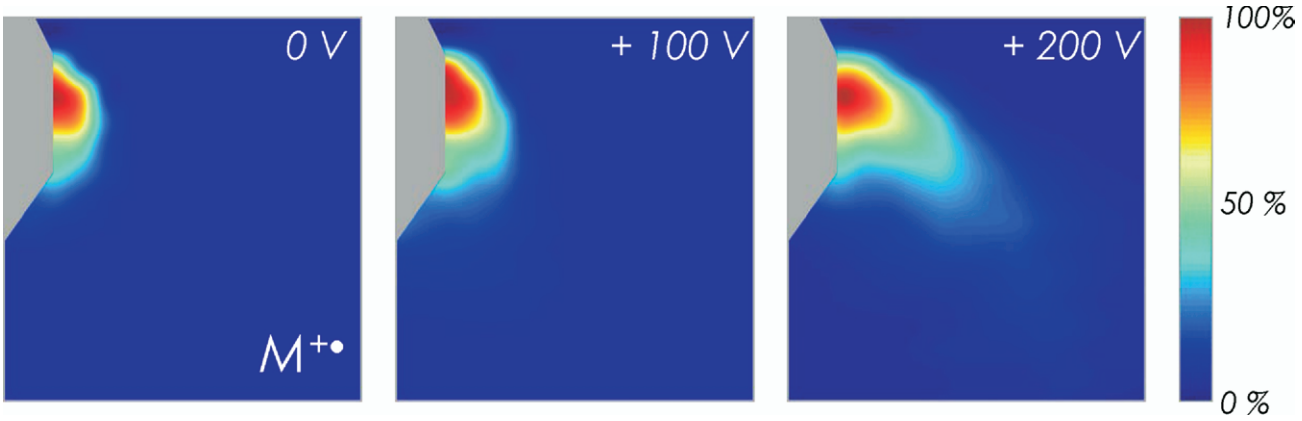

Figure 5. Pseudo-color plots of the spatially resolved signal response for $M^{\cdot+}$ (m/z 166) of 1 μmol L^{-1} fluorene in CH_3CN. From left to right the repeller voltage is increased as shown. Vertical scale: 15 mm, horizontal scale: 14 mm. Each plot is based on a color scale relative to the maximum signal in each plot, as shown on the right.

detected only in close vicinity to the sampling orifice, whereas the maximum signal intensity of $[M + H]^+$ is located at larger distances up to 10 mm from the sampling orifice, as shown in Figure 6a and b, respectively, and (3) the contribution of quasimolecular ions to the DIAV of DMBA is much larger.

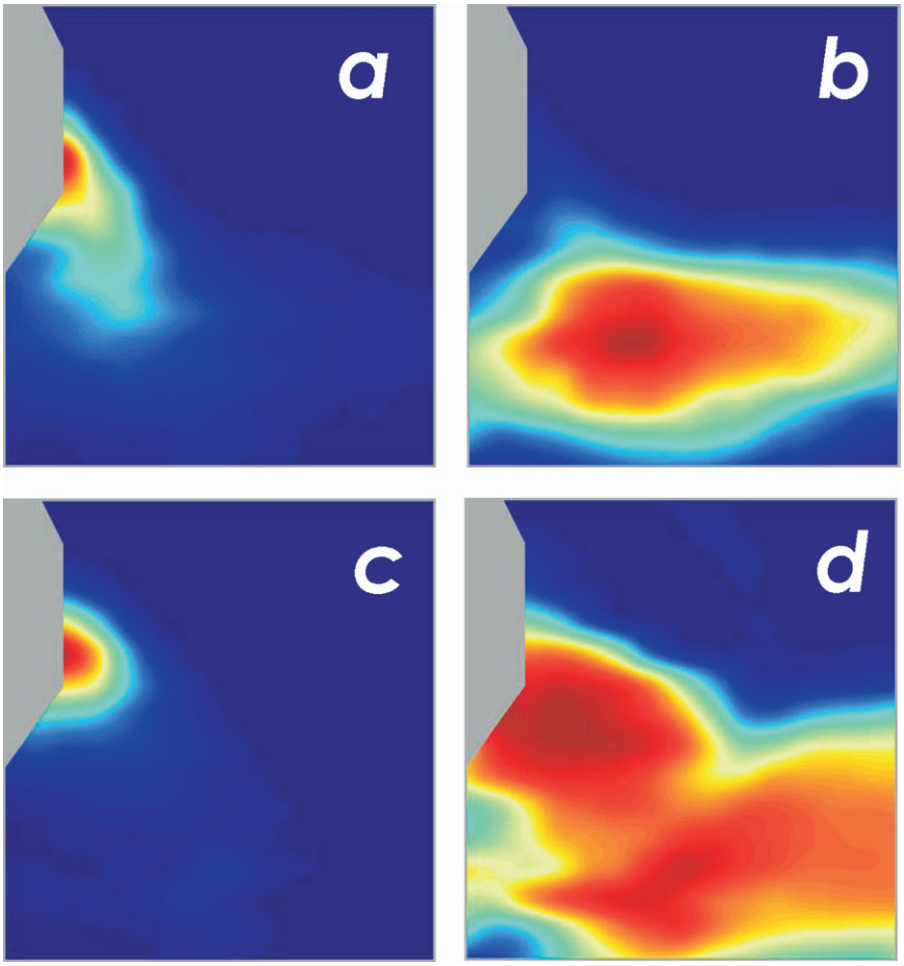

Figure 6. Spatially resolved measurements of the signal response of 10 μmol L^{-1} DMBA dissolved in *n*-heptane. (**a**) $M^{\cdot+}$ (m/z 257) signal. (**b**) $[M + H]^+$ signal. (**c**) and (**d**) $M^{\cdot+}$ and $[M + H]^+$ signal, respectively, after addition of 0.1% (by volume) toluene as dopant. See text for details. Color scale: See Figure 5.

Due to the large gas-phase basicity of DMBA, addition of a dopant acting as proton donor should increase the bulk $[M + H]^+$ signal intensity, as has been verified in separate experiments. In APLI a proton donor is easily generated similar to the approach discussed above for APPI. Upon addition of a dopant, in the present case a 1000-fold excess of toluene over DMBA, spatially resolved measurements show that the DIAV broadens considerably due to the contribution of the quasimolecular ions and extends all the way to the sampling orifice (see Figure 6d). It is emphasized that the contribution of $M^{\cdot+}$ remains largely unaffected by the dopant induced ion chemistry.

Upon raising the molecular oxygen content of the main gas flow up to 20% by volume, the DIAV contribution of $M^{\cdot+}$ is significantly reduced in size by a factor of 3 to 6; the corresponding contribution of $[M + H]^+$, however, is far less affected, if at all.

Discussion

Analysis of DIA and DIAV Measurements

As expected, radical cations are always detectable in high yield close to the sampling orifice of the MS; this illustrates the direct nature of the ion generation process. The observed contribution to an analyte's DIAV, however, is generally much smaller compared with that of quasimolecular ions. This clearly demonstrates that the mass analyzer is capable of accepting ions from a relatively large volume within the API source; in the present set-up, ions appear to be forced through the sampling nozzle mostly by fluid flow dynamics and to a lesser extent by electrical field gradients. The presented data further suggest that radical cations of *nonpolar* compounds react swiftly away within the matrix to yield neutral reaction products since no other significant mass signals were detectable within the analyzer mass range ($100 < m/z < 1000$). One possible fate of $M^{\cdot+}$ is deprotonation via Reactions 4 and 5 ($D \equiv M$). However, similar results were observed for CH_3CN and *n*-heptane as solvent. In the latter case, cluster formation is far less favorable. The measured adverse impact of O_2 on the DIA of $M^{\cdot+}$ to yield mainly uncharged products is proposed to originate from *termolecular* ion-molecule recombination reactions of the type

$$M^{\cdot+} + \cdot O_2 \cdot + N_2 \rightarrow \left[M + O_2\right]^{\cdot+} + N_2 \qquad (7)$$

followed by fast subsequent loss of charge via fragmentation and/or proton loss of the adduct. It is noted that *bimolecular* radical cation-O_2 reactions are usually rather slow [41] to account for the observed ion signal intensity losses.

The time scale for the passage of an ion generated at a distance of 10 mm to reach the nozzle is about 15 ms assuming that the gases enter the source enclosure as a laminar flow. During this time, individual radical cations have undergone about 10^8 collisions, as estimated from kinetic gas theory. Provided the speculated loss reaction is fast, even very small amounts of O_2 impurities could significantly deplete the original radical cation population. In contrast hereto, quasimolecular ions are basically not reacting with molecular oxygen neither in bimolecular nor termolecular channels [41]. Thus, the observed loss in polar as well as nonpolar solvents is rather low. Most LC-MS use high-flow nitrogen generators for continuous operation; in this case, O_2 mixing ratios up to 0.5% per volume can be expected to be present within the ion source enclosure.

The unexpected formation of quasimolecular ions in APPI has been discussed by Syage [18] using a combined thermodynamic and kinetic approach; in this model, the equilibrium (eqs 8a, b) is shifted towards the product side due to the large excess of solvent molecules:

$$M^{\cdot+} + S \leftrightarrows \left[M + H\right]^+ + \left[S - H\right]^{\cdot} \qquad (8a,b)$$

The same conclusion is drawn in the present work since the formation of quasimolecular ions appears to be delayed with respect to the laser pulse arriving in the source (cf. Figure 6b). In the vicinity of the nozzle, lower $[M + H]^+$ concentrations were detectable, suggesting that equilibrium was not reached; at higher distances and thus reactions times, the maximum signal intensity covers a broad plateau region.

The addition of a dopant induces another means of analyte charging by proton transfer as has been discussed; cf. eqs 2–5. This process appears to be much faster than the H-abstraction route (eq 8a): Figure 6d shows a significant shift of the DIAV due to the contribution of $[M + H]^+$ towards the nozzle and thus shorter reaction times.

APPI versus APLI Ionization Mechanism

The above very simple model allows to account for the observed differences in APPI versus APLI, particularly the poor detection limits reported for non-polar PAH measurements in APPI. Figure 7 shows two contour plots for (Figure 7a) B*a*P forming the molecular ion only and (Figure 7b) nicotine forming the quasimolecular ion only at LC conditions, respectively. The light penetration depth, expressed as $I/I_0 \geq 2\%$ (intensity I, initial light intensity I_0, cf. Results section) of the 124 nm VUV radiation entering from the right in APPI is colored in yellow; the blue area indicates the laser irradiated area in APLI mode. The intensity of the VUV light drops to virtually zero at distances of a few mm from the lamp window, not taking into account the presence of molecular oxygen. Although most LC solvents as well as N_2 and O_2 do not directly ionize at 124 nm, with the exception of nitrogen all compounds strongly absorb at this wavelength. Assuming typical LC-MS conditions, the relative VUV light intensity I/I_0 has been shown (cf. Results section) to drop to drop below 10% at a distance of about 2 mm from the lamp surface. The $M^{\cdot+}$ contour

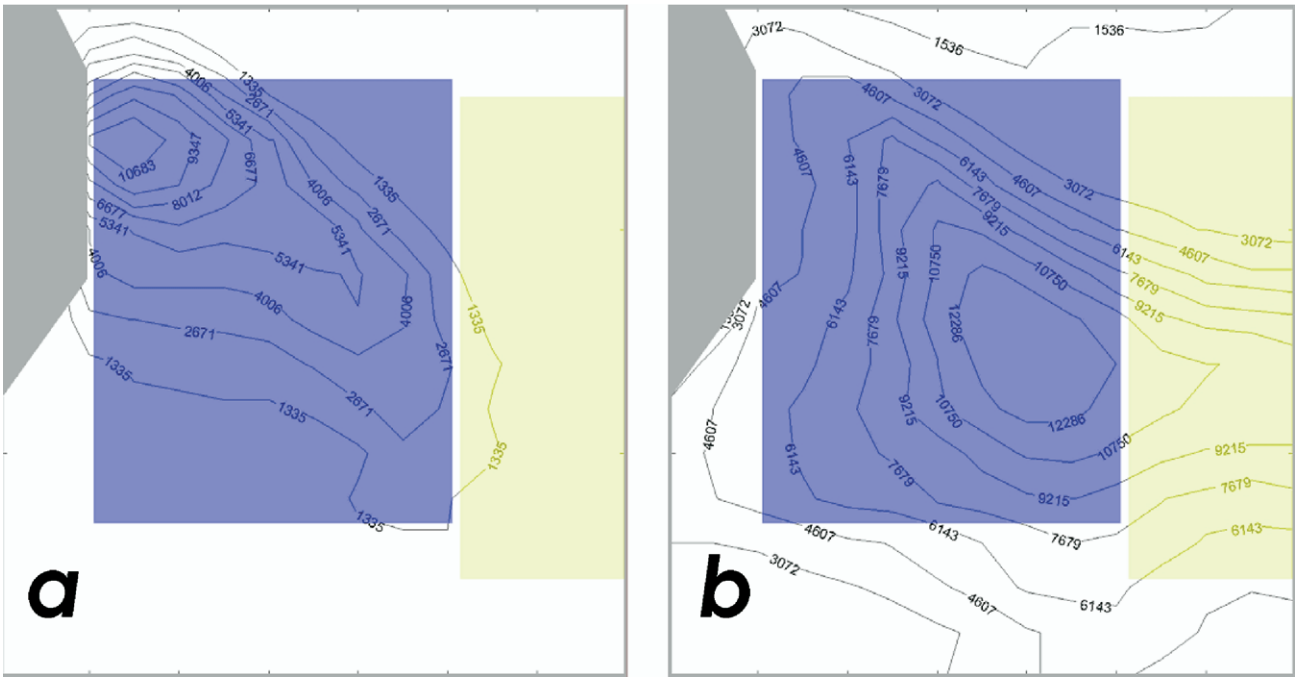

Figure 7. Contour plots of the spatially resolved signal response for $M^{\cdot+}$ of B*a*P (*m/z* 252, left panel) and $[M + H]^+$ of nicotine (*m/z* 163, right panel) dissolved in CH_3CN. The isolines are shown for MS counts. Yellow area: VUV light intensity $I/I_0 \geq 2\%$. The VUV emitting surface is located at the right plot boundary. Blue area: Typical laser beam cross section (entering from above) used in APLI. See text for details.

plot clearly shows that primary radical cations photochemically formed at the corresponding distance of about 10 mm to the nozzle have nearly quantitatively reacted away before entering the analyzer region. Possible fates of the radical cations are discussed above; nonpolar compounds such as PAH are most probably neutralized, whereas compounds with high gas-phase basicities are converted to quasimolecular ions through interaction with solvent molecules.

In APLI the absorption of the laser radiation by matrix compounds at 248 nm is virtually negligible. The UV laser light thus fully penetrates the ion source region. The irradiated region includes both, the DIAV-contributions from $M^{\cdot+}$ as well as from $[M + H]^+$. Thus, nonpolar compounds are generally detected as radical cations; in this case the laser radiation is preferentially directed close to the nozzle orifice. Quasimolecular ion generation is observed for polar analytes by H-abstraction of the primarily formed radical cations from the solvent (slow) or by proton transfer to the neutrals in the presence of a dopant (fast). In this case the laser radiation is preferentially directed further away from the nozzle through the effluent from the vaporization stage.

Conclusion

Spatially resolved measurements of the signal response in an AP ion source are presented for the first time. This application of APLI represents a powerful tool for AP ion source optimization with respect to geometry, electrical field gradients, and flow dynamics, particularly in combination with simulation program packages such as ion trajectory calculations and computational fluid dynamics. Furthermore, mechanistic studies of hitherto unprecedented detail are possible. Both applications are demonstrated in the present paper. With respect to the speculated different ionization mechanisms in APLI versus APPI, it is shown that the apparent lack of sensitivity of APPI towards detection of radical cations of nonpolar compounds is mainly due to absorption of the VUV light by matrix compounds; both photo ionization techniques generate primarily radical cations and the suspected differences in the ionization mechanisms are readily explained by the different position of primary ion formation and subsequent ion-molecule chemistry.

Acknowledgments

The authors thank the reviewers of this manuscript for their constructive and very helpful input.

References

1. Niessen, W. M. A. Progress in Liquid Chromatography-Mass Spectrometry Instrumentation and Its Impact on High-Throughput Screening. *J. Chromatogr. A* **2003,** *1000,* 413–436.
2. Niessen, W. M. A. LC-MS in Quantitative Analysis. *Rev. Anal. Chem.* **2000,** *19,* 289–301.
3. Niessen, W. M. A. State-of-the-Art in Liquid Chromatography-Mass Spectrometry. *J. Chromatogr. A* **1999,** *856,* 179–197.
4. Bos, S. J.; van Leeuwen, S. M.; Karst, U. From Fundamentals to Applications: Recent Developments in Atmospheric Pressure Photoionization Mass Spectrometry. *Anal. Bioanal. Chem.* **2006,** *384,* 85–99.

5. Van Berkel, G. J. An Overview of Some Recent Developments in Ionization Methods for Mass Spectrometry. *Eur. J. Mass Spectrom.* **2003,** 9539–562.
6. Raffaelli, A.; Saba, A. Atmospheric Pressure Photoionization Mass Spectrometry. *Mass Spectrom. Rev.* **2003,** *22,* 318–331.
7. Constapel, M.; Schellenträger, M.; Schmitz, O. J.; Gäb, S.; Brockmann, K. J.; Giese, R.; Benter, T. Atmospheric Pressure Laser Ionization: A Novel Ionization Method for Liquid Chromatography/Mass Spectrometry. *Rapid Commun. Mass Spectrom.* **2005,** *19,* 326–336.
8. Droste, S.; Schellenträger, M.; Constapel, M.; Gäb, S.; Lorenz, M.; Brockmann, K. J.; Benter, T.; Lubda, D.; Schmitz, O. J. A Silica-Based Monolithic Column in Capillary HPLC and CEC Coupled with ESI-MS or Electrospray-Atmospheric-Pressure Laser Ionization-MS. *Electrophoresis* **2005,** *26,* 4098–4103.
9. Benter, T.; Schmitz, O. J. Atmospheric Pressure Laser Ionization. In *Advances in LC-MS Instrumentation. Journal of Chromatography Library* 72; Cappiello, A. Ed.; Elsevier: Amsterdam, The Netherlands, 2007; p 89.
10. Benter, T. Atmospheric Pressure Laser Ionization. In *The Encyclopedia of Mass Spectrometry* 1st ed.; Gross, M. L., Caprioli, R. N. Eds., Elsevier: Oxford, U.K., 2007; p 251.
11. Schiewek, R.; Schellentrager, M.; Monnikes, R.; Lorenz, M.; Giese, R.; Brockmann, K. J.; Gäb, S.; Benter, T.; Schmitz, O. J. Ultrasensitive Determination of Polycyclic Aaromatic Compounds with Atmospheric-Pressure Laser Ionization as an Interface for GC/MS. *Anal. Chem.* **2007,** *79,* 4135–4140.
12. Syage, J. A.; Hanning-Lee, M. A.; Hanold, K. A. A Man-Portable, Photoionization Time-of-Flight Mass Spectrometer. *Field Anal. Chem. Technol.* **2000,** *4,* 204–215.
13. Syage, J. A.; Evans, M. D.; Hanold, K. A. Photoionization Mass Spectrometry. *Am. Lab.* **2000,** *32,* 24–29.
14. Robb, D. B.; Blades, M. W. Effects of Solvent Flow, Dopant Flow, and Lamp Current on Dopant-Assisted Atmospheric Pressure Photoionization (DA-APPI) for LC-MS Ionization via Proton Transfer. *J. Am. Soc. Mass Spectrom.* **2005,** *16,* 1275–1290.
15. Robb, D. B.; Covey, T. R.; Bruins, A. P. Atmospheric Pressure Photoionization: An Ionization Method for Liquid Chromatography-Mass Spectrometry. *Anal. Chem.* **2000,** *72,* 3653–3659.
16. Robb, D. B.; Blades, M. W. Factors Affecting Primary Ionization in Dopant-Assisted Atmospheric Pressure Photoionization (DA-APPI) for LC/MS. *J. Am. Soc. Mass Spectrom.* **2006,** *17,* 130–138.
17. Kauppila, T. J.; Bruins, A. P.; Kostiainen, R. Effect of the Solvent Flow Rate on the Ionization Efficiency in Atmospheric Pressure Photoionization-Mass Spectrometry. *J. Am. Soc. Mass Spectrom.* **2005,** *16,* 1399–1407.
18. Syage, J. A. Mechanism of $[M + H]^+$ Formation in Photoionization Mass Spectrometry. *J. Am. Soc. Mass Spectrom.* **2004,** *15,* 1521–1533.
19. Kauppila, T. J.; Kotiaho, T.; Kostiainen, R.; Bruins, A. P. Negative Ion-Atmospheric Pressure Photoionization-Mass Spectrometry. *J. Am. Soc. Mass Spectrom.* **2004,** *15,* 203–211.
20. Kauppila, T. J.; Kostiainen, R.; Bruins, A. P. Anisole, a New Dopant for Atmospheric Pressure Photoionization Mass Spectrometry of Low Proton Affinity, Low Ionization Energy Compounds. *Rapid Commun. Mass Spectrom.* **2004,** *18,* 808–815.
21. Tubaro, M.; Marotta, E.; Seraglia, R.; Traldi, P. Atmospheric Pressure Photoionization Mechanisms. 2. The Case of Benzene and Toluene. *Rapid Commun. Mass Spectrom.* **2003,** *17,* 2423–2429.
22. Marotta, E.; Seraglia, R.; Fabris, F.; Traldi, P. Atmospheric Pressure Photoionization Mechanisms. 1. The Case of Acetonitrile. *Int. J. Mass Spectrom.* **2003,** *228,* 841–849.
23. Lorenz, M.; Brockmann, K. J.; Schiewek, R.; Constapel, M.; Schmitz, O. J.; Gäb, S.; Benter, T. On the Ionization Mechanisms in APPI versus APLI. *Proceedings of the 54th ASMS Conference on Mass Spectrometry and Allied Topics*; Seattle, WA, May, 2006.
24. Chernushevich, I. V.; Loboda, A. V.; Thomson, B. A. An Introduction to Quadrupole-Time-of-Flight Mass Spectrometry. *J. Mass Spectrom.* **2001,** *36,* 849–865.
25. Boesl, U. Special Feature: Tutorial—Laser Mass Spectrometry for Environmental and Industrial Chemical Trace Analysis. *J. Mass Spectrom.* **2000,** *35,* 289–304.
26. Pfab, J. Laser-Induced Fluorescence and Ionization Spectroscopy of Gas Phase Species. In *Spectroscopy in Environmental Science*; Clark, R. J. H.; Hester, R. E., Eds.; John Wiley and Sons: New York, 1995; p 149.
27. Ashfold, M. N. R.; Howe, J. D. Multiphoton Spectroscopy of Molecular Species. *Annu. Rev. Phys. Chem.* **1994,** *45,* 57–82.
28. Muehlberger, F.; Zimmermann, R.; Kettrup, A. A Mobile Mass Spectrometer for Comprehensive On-Line Analysis of Trace and Bulk Components of Complex Gas Mixtures: Parallel Application of the Laser-Based Ionization Methods VUV Single-Photon Ionization, Resonant Multiphoton Ionization, and Laser-Induced Electron Impact Ionization. *Anal. Chem.* **2001,** *73,* 3590–3604.
29. Cao, L.; Muehlberger, F.; Adam, T.; Streibel, T.; Wang, H. Z.; Kettrup, A.; Zimmermann, R. Resonance-Enhanced Multiphoton Ionization and VUV-Single Photon Ionization as Soft and Selective Ionization Methods for On-Line Time-of-Flight Mass Spectrometry: Investigation of the Pyrolysis of Typical Organic Contaminants in the Steel Recycling Process. *Anal. Chem.* **2003,** *75,* 5639–5645.
30. Burton, G. R.; Chan, W. F.; Cooper, G.; Brion, C. E. Absolute Oscillator-Strengths for Photoabsorption (6-360 eV) and Ionic Photofragmentation (10-80 eV) of Methanol. *Chem. Phys.* **1992,** *167,* 349–367.
31. Burton, G. R.; Chan, W. F.; Cooper, G.; Brion, C. E. The Electronic Absorption Spectrum of NH_3 in the Valence Shell Discrete and Continuum Regions—Absolute Oscillator-Strengths for Photoabsorption (5–200 eV). *Chem. Phys.* **1993,** *177,* 217–231.
32. Chan, W. F.; Cooper, G.; Brion, C. E. The Electronic-Spectrum of Water in the Discrete and Continuum Regions—Absolute Optical Oscillator-Strengths for Photoabsorption (6–200 eV). *Chem. Phys.* **1993,** *178,* 387–400.
33. Cooper, G.; Anderson, J. E.; Brion, C. E. Absolute Photoabsorption and Photoionization of Formaldehyde in the VUV and Soft X-Ray Regions (3–200 eV). *Chem. Phys.* **1996,** *209,* 61–77.
34. Eden, S.; Limao-Vieira, P.; Kendall, P.; Mason, N. J.; Hoffmann, S. V.; Spyrou, S. M. High Resolution Photoabsorption Studies of Acrylonitrile, C_2H_3CN, and Acetonitrile, CH_3CN. *Eur. Phys. J. D* **2003,** 26, 201–210.
35. Au, J. W.; Cooper, G.; Burton, G. R.; Olney, T. N.; Brion, C. E. The Valence Shell Photoabsorption of the Linear Alkanes, C_nH_{2n+2}(n = 1–8)– Absolute Oscillator-Strengths (7–220 eV). *Chem. Phys.* **1993,** *173,* 209–239.
36. Cristoni, S.; Bernardi, L. R.; Guidugli, F.; Tubaro, N.; Traldi, P. The Role of Different Phenomena in the Surface-Activated Chemical Ionization (SACI) Performance. *J. Mass Spectrom.* **2005,** *40,* 1550–1557.
37. Demtröder, W. *Laser Spectroscopy*, 3rd ed.; Springer: New York, 2002; p 207.
38. Johnson, P. M.; Otis, C. E. Molecular Multiphoton Spectroscopy with Ionization Detection. *Annu. Rev. Phys. Chem.* **1981,** *32,* 139–157.
39. Zakheim, D. S.; Johnson, P. M. Rate-Equation Modeling of Molecular Multiphoton Ionization Dynamics. *Chem. Phys.* **1980,** *46,* 263–272.
40. Hunter, E. P., Lias, S. G., Proton Affinity Evaluation. In *NIST Chemistry WebBook,* NIST Standard Reference Database Number 69; Linstrom, P. J.; Mallard, W. G., Eds.; National Institute of Standards and Technology: Gaithersburg MD, 20899 (http://webbook.nist.gov) 2005.
41. Anicich, V. G. *An Index of the Literature for Bimolecular Gas Phase Cation-Molecule Reaction Kinetics*, JPL Publications; California Institute of Technology: Pasadena, CA, 2003.